

# Short Paper

## Modeling of Slip for Wheeled Mobile Robots

R. Balakrishna and Ashitava Ghosal

**Abstract**—Wheeled Mobile Robots (WMRs) are known to be non-holonomic systems, and most dynamic models of WMRs assume that the wheels undergo rolling without slipping. This paper deals with the problem of modeling and simulation of motion of a WMR when the conditions for rolling are not satisfied at the wheels. We use a traction model where the adhesion coefficient between the wheels of a WMR and a hard flat surface is a function of the wheel slip. This traction model is used in conjunction with the dynamic equations of motion to simulate the motion of the WMR. The simulations show that controllers which do not take into account wheel slip give poor tracking performance for the WMR and path deviation is small only for large adhesion coefficients. This work shows the importance of wheel slip and suggests use of accurate traction models for improving tracking performance of a WMR.

**Index Terms**—Wheeled Mobile Robots, Slip, Modeling, Traction, Adhesion.

### I. INTRODUCTION

Wheeled Mobile Robots (WMRs) are generally modeled as non-holonomic dynamical systems with its wheels assumed to be rolling without slipping. The formulation based on rolling without slip gives kinematical mappings between wheel rotation and the position and orientation of the WMR. However, rolling conditions are sometimes violated in tractive maneuvering of WMRs, predominantly due to slipping and scrubbing [3]. In this paper, we use a model for the tractive force in terms of the adhesion coefficient, the linear and angular velocity of the wheel. The dynamic equations of motion are then derived including the effect of the tractive forces. It is shown that the equations of motion reduce to that obtained for 'ideal' rolling when no slip conditions are used. The 'ideal' rolling model is used to develop a model based controller. Simulation results with a PID controller and the model based controller show that the unmodeled slipping results in significant path deviation for the WMR, especially when adhesion coefficients are small. Hence, to obtain realistic models for maneuvering of WMRs, the rigid body dynamics of the WMR needs to be used in conjunction with slipping and tractive forces at the wheel-surface contact.

Previous work in wheeled mobile robot modeling have neglected the aspect of wheel slip [1], [2], [19]. Other studies examined WMR maneuvering by considering the case when the torque applied does not exceed the traction limit [14]. The work presented by Alexander and Maddocks [3] predicts the resulting motion of a WMR by minimizing a friction functional when scrubbing takes place. Muir and Neuman [11], [12] describe methods to detect wheel slip and describe corrective measures.

The modeling of tractive forces developed at the wheel has been used for various studies [18], [4], [8]. The model presented here has been widely used for automobile dynamic stability analysis [8], [17] and for traction control [16]. We discuss the model for wheel slip in Section 2.

Manuscript received April 13, 1993; revised November 24, 1993.

The author is with the Department of Mechanical Engineering, Indian Institute of Science, Bangalore 560 012 India.

IEEE Log Number 9404617.

The mechanical configuration of WMRs falls into one of two categories – steered-wheeled vehicles and differential-drive vehicles. This paper uses the latter category for simulation studies [9].

This paper is organized as follows: Section 2 presents the notion of wheel slip and wheel dynamics, Section 3 presents the Adhesion Coefficient model, Section 4 presents the WMR dynamic model with the wheel slip incorporated and control of the WMR is considered in Section 5. In Section 6 simulations for a 3 wheeled omni-wheeled mobile robot is discussed and in Section 7 we present our conclusions.

### II. WHEEL-SLIP AND SINGLE WHEEL DYNAMICS

For a conventional wheel, the linear velocity of the wheel center,  $v$ , and wheel angular velocity,  $\omega$ , are related through the expression,  $v = r \omega$ , where  $r$  is the wheel radius. This expression represents 'ideal' rolling. This relation is a nonholonomic constraint between the variables  $v$  and  $\omega$ . When the wheel rolls with slip this constraint is violated.

To determine wheel slip between the wheel and a hard surface, it is assumed that the surface does not deform during traction but the wheel may undergo deformation at the contact patch. The wheel slip,  $\lambda$ , can be defined as

$$\lambda = (\dot{\theta} - \omega^*) / y \quad (1)$$

where,  $\omega^*$  is defined as  $v/r$  with units of rad/sec, and  $\dot{\theta}$  is the wheel angular velocity in rad/sec. The value of  $y$  is  $\omega^*$  when  $\omega^* > \dot{\theta}$  and is  $\dot{\theta}$  when  $\omega^* < \dot{\theta}$ .

It may be observed that  $-1 \leq \lambda \leq 1$ . For 'ideal' rolling, when  $\omega^* = \dot{\theta}$ , the wheel slip  $\lambda$  is zero. When the linear velocity is zero,  $\lambda = 1$ , and this represents the condition of wheel angular acceleration and rolling in place. The skid condition is characterized by zero angular velocity while the vehicle possesses a linear velocity. In this case  $\lambda = -1$ .

To represent the combined effects of rolling and slipping, the tractive forces of the wheel have to be introduced. The translational and rotational dynamics of a wheel of radius  $r$ , mass  $M_w$ , and moment of inertia about the wheel center  $J_w$ , can be written as

$$\begin{aligned} F_t &= M_w \ddot{x} \\ \tau &= J_w \ddot{\theta} + F_t r \end{aligned} \quad (2)$$

where,  $F_t$ , is the tractive force developed at the wheel contact,  $\ddot{x}$  and  $\ddot{\theta}$  are the linear and angular acceleration of the wheel center, respectively, and  $\tau$  is the torque applied at the wheel axle. The above equations of motion for a single wheel undergoing roll/slip motion may be expressed in the state space form. Using the state vector,  $\mathbf{x} = \{x_1, x_2, x_3, x_4\}^T$ , to represent the Cartesian position, linear velocity, angular rotation and angular velocity, respectively, we can write (2) as

$$\begin{pmatrix} \dot{x}_1 \\ \dot{x}_2 \\ \dot{x}_3 \\ \dot{x}_4 \end{pmatrix} = \begin{pmatrix} x_2 \\ F_t/M_w \\ x_4 \\ -r F_t/J_w \end{pmatrix} + \begin{pmatrix} 0 \\ 0 \\ 0 \\ 1/J_w \end{pmatrix} \tau$$

or compactly as,

$$\dot{\mathbf{x}} = \underline{f}(\mathbf{x}) + \underline{g} \tau. \quad (3)$$

It can be observed that the translational and rotational dynamics for a wheel undergoing roll/slip motion are coupled through the tractive force  $F_t$ . It should be noted that the torque,  $\tau$ , is the only external independent input to this dynamical system.

For this system to be locally controllable (see Isidori [10], Spong and Vidyasagar [15]), the following vectors  $\{\underline{g}, ad_{\underline{f}}(\underline{g}), ad_{\underline{f}}^2(\underline{g}), ad_{\underline{f}}^3(\underline{g})\}$  should be linearly independent.<sup>1</sup> One can show that  $ad_{\underline{f}}^2(\underline{g})$  becomes a zero vector if  $F_t$  is constant. Hence for the vectors to be linearly independent, the tractive force  $F_t$  should be at least a  $C^1$  continuous function in  $x_2$  and  $x_4$ , which are the linear and angular velocities of the wheel. In the next section a traction model including the effects of wheel roll/slip will be described.

### III. ADHESION COEFFICIENT MODEL

The adhesion coefficient [16] has also been referred to as the "friction coefficient" for wheel rolling [8], and generally used as a measure to determine the adhesivity or sticking between two surfaces. The tractive force,  $F_t$ , is generally obtained by the product of the adhesion coefficient and normal force at the point of contact. The adhesion coefficient is a function of the wheel dynamics and tractive conditions. It depends on quantities such as linear velocity of the wheel, the angular velocity of the wheel and the surface roughness in qualitative and quantitative aspects. Various models have been proposed for the tractive force,  $F_t$ , in literature [4], [18], [8]. Unruh [18] uses a model where the adhesion coefficient is assumed to be constant while Allen and O'Massey [4] assume a model where the adhesion coefficient is a function of the linear velocity. These models are useful only when the wheel is locked and the vehicle is skidding. We have used the traction model as proposed by Dugoff *et al.* [8]. The models presented here are for longitudinal wheel traction force.

#### Adhesion Coefficient Dependent on Wheel Slip

In the model proposed by Dugoff *et al.* [8], the tractive force,  $F_t$ , is a function of wheel slip,  $\lambda$  (see Section 2). The tractive force,  $F_t$ , is given by  $\mu_a N$ , where  $\mu_a$  is the adhesion coefficient and  $N$  is the normal reaction.  $\mu_a$  depends on the wheel slip,  $\lambda$ , which in turn is a function of linear and angular velocities of the wheel. The tractive force developed is then formulated as

$$F_t = \mu_a(\lambda) N \quad (4)$$

The relation between the adhesion coefficient,  $\mu_a$ , and wheel slip,  $\lambda$ , depends on the nature of the surface and the wheel material [8]. A typical relationship is shown in Fig. 1 which shows the change in adhesion coefficient,  $\mu_a$ , for acceleration and braking conditions. This curve has been proposed and verified by Dugoff *et al.* [8]. For a given surface and wheel material, it has been observed that though the quantitative characteristic of the curve may change, it matches qualitatively for different surfaces. Of particular significance is the peak value  $\mu_{a_{peak}}$  (shown in Fig. 1), which is present for the acceleration and braking regions, with  $\lambda$  taking positive and negative values, respectively.

The adhesion coefficient,  $\mu_a$ , shows a rise and then a fall with increasing wheel-slip,  $\lambda$ , where  $0 \leq |\lambda| \leq 1$ . The stable region is represented by the portion of the curve that shows an increase in the  $\mu_a$  with increase in  $\lambda$ . In this portion, the tractive forces that can be sustained increases with the wheel-slip due to the increase in  $\mu_a$ . The fall of  $\mu_a$  beyond the peak  $\mu_{a_{peak}}$  results in instability since the tractive force reduces with increasing slip [16].

<sup>1</sup> $ad_{\underline{f}}(\underline{g})$  denotes the Lie Bracket of the two vector fields  $\underline{f}$  &  $\underline{g}$  with  $ad_{\underline{f}}^k(\underline{g}) = [\underline{f}, ad_{\underline{f}}^{k-1}(\underline{g})]$  and  $ad_{\underline{f}}^0(\underline{g}) = \underline{g}$ .

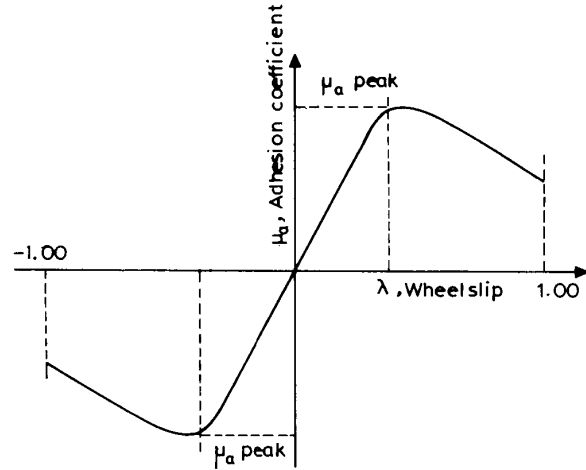


Fig. 1.  $\mu$  versus  $\lambda$  curve.

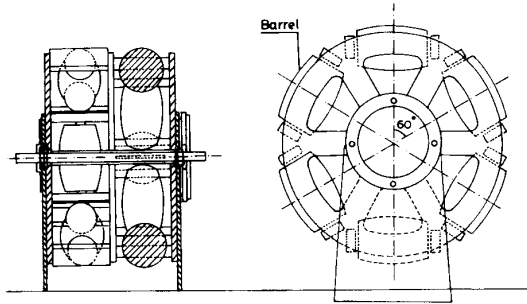


Fig. 2. An Omni-wheel.

It was observed in Section 2, that the controllability of a wheel is ensured if the tractive force model,  $F_t$ , is at least  $C^1$  continuous in  $x_2$  and  $x_4$ . The present adhesion coefficient model based on wheel-slip satisfies this criterion and also enables the representation of combined rolling and slipping in the wheel. In view of the above mentioned factors this adhesion coefficient model was used in the simulations.

The lateral tractive force model for the wheel is not considered here, because the WMR considered in this work is a differential drive vehicle with omni-wheels. However, lateral tractive force can also be considered along similar lines [8], [17].

### IV. WMR DYNAMIC MODEL WITH WHEEL SLIP

The omni-wheel has freely rotating barrels at the periphery and the axis of rotation of the barrels are at an angle to the axis of rotation of the wheel. Thus, they have two degrees of freedom as opposed to conventional wheels which have one degree of freedom [1], [11]. We consider a planar WMR with three omni-wheels and with barrels inclined at  $90^\circ$  to the wheel axis [9]. To ensure that the wheel always has two degrees of freedom, we consider a wheel having two layers of barrels as shown in Fig. 2. The kinematic and dynamics of WMRs (assuming no slip) with more than three wheels and with barrels inclined at other angles can also be derived [1], [2].

For the planar WMR with three omni-wheels placed at an angular separation of  $120^\circ$ , shown in Fig. 3, one can find the relationship between the wheel variables and the Cartesian variables by using the no slip condition at the three wheels. Let the wheel rotational speeds,  $\{\theta_1, \theta_2, \theta_3\}$ , be denoted by  $\underline{\theta}$ , the wheel sliding speeds,

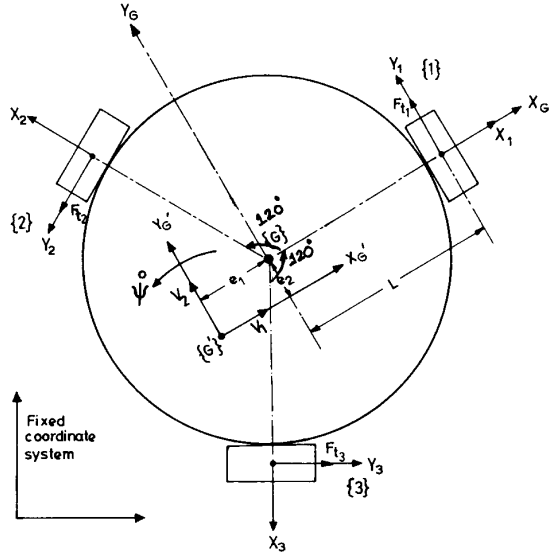


Fig. 3. WMR with coordinate frames and forces

$\{\sigma_1, \sigma_2, \sigma_3\}$ , be denoted by  $\underline{\sigma}$ . Since the motion of the WMR is in a plane, the velocity of any point  $G'$  (origin of the body fixed frame  $\{G'\}$ ) on the WMR, with respect to a fixed coordinate system, can be described by two components,  $\{V_1, V_2\}$ , and the angular velocity of the WMR can be described by a single component  $\dot{\Psi}$  normal to the platform. It may be noted that  $\{V_1, V_2\}$ , as shown in Fig. 3, are along  $X_{G'}$  and  $Y_{G'}$  axes, respectively. We denote  $\{V_1, V_2, \dot{\Psi}\}$  by  $\underline{V}$ . It can be shown [1], that  $\underline{\dot{\theta}}$  and the Cartesian variables,  $\underline{V}$ , are related by

$$\begin{Bmatrix} \dot{\theta}_1 \\ \dot{\theta}_2 \\ \dot{\theta}_3 \end{Bmatrix} = \frac{1}{r} \begin{bmatrix} 0 & 1 & L_1 \\ -\sqrt{3}/2 & -1/2 & L_2 \\ \sqrt{3}/2 & -1/2 & L_3 \end{bmatrix} \begin{Bmatrix} V_1 \\ V_2 \\ \dot{\Psi} \end{Bmatrix} = [R] \begin{Bmatrix} V_1 \\ V_2 \\ \dot{\Psi} \end{Bmatrix} \quad (5)$$

where,  $r$  is the omniscience wheel radius and  $L_i$ ,  $i = 1, 2, 3$  are the distances of the omniscience wheel contact point from  $G'$ . The  $[R]$  matrix relates  $\underline{\dot{\theta}}$  and  $\underline{V}$  and is analogous to Jacobian matrix in manipulators. The relationship between the sliding velocity of the omniscience wheels,  $\underline{\sigma}$ , and the Cartesian velocities has been presented by Agullo *et al.* [1].

When the platform is rolling without slipping it has 3 degrees of freedom. However, when the rolling constraint is not satisfied, the WMR system has six degrees of freedom described by  $\{X, Y, \Psi\}$  and  $\{\theta_1, \theta_2, \theta_3\}$ . This is because the  $\theta$ 's and  $V_1, V_2, \dot{\Psi}$  are not related through the kinematic relations for 'ideal' rolling shown in (5).

Let  $G$  be the center of mass of the WMR. The frame  $\{G\}$  is aligned to the frame  $\{G'\}$  and has coordinates  $(e_1, e_2)$  with respect to  $\{G'\}$  as shown in Fig. 3. The velocity of the center of mass, with respect to a fixed frame, can be written as

$$\underline{V}_G = \{V_1 - \dot{\Psi} e_2, V_2 + \dot{\Psi} e_1\}^T. \quad (6)$$

Let  $M_p$  be the mass of the WMR,  $I_p$  be the moment of inertia of the WMR about  $Z$  axis,  $I_i$  the moment of inertia of each wheel about its axis, and  $r$  the radius of each omniscience wheel. The kinetic energy of the WMR is given by the wheel rotational energy, and the WMR translational and rotational energies. The kinetic energy contribution of the barrels on the omniscience wheel are neglected. The Lagrangian for the WMR is given as

$$\mathcal{L} = \frac{1}{2} \{M_p \underline{V}_G \cdot \underline{V}_G + I_p \dot{\Psi}^2 + \sum_{i=1}^3 I_i \dot{\theta}_i^2\}. \quad (7)$$

Using the Lagrangian formulation, we can derive the equations of motion for WMR systems as

$$\frac{d}{dt} \left\{ \frac{\partial \mathcal{L}}{\partial \dot{q}_j} \right\} - \frac{\partial \mathcal{L}}{\partial q_j} = \mathcal{F}_j, \quad j = 1, \dots, 6 \quad (8)$$

where,  $\mathcal{L}$ , is the Lagrangian of the WMR given in (7),  $q_j$ ,  $i = 1, \dots, 6$  is the set  $\{X, Y, \Psi, \theta_1, \theta_2, \theta_3\}$  of generalized coordinates, and  $\mathcal{F}$  are the generalized forces.

The generalized forces corresponding to  $\theta_i$ ,  $i = 1, 2, 3$  are  $\tau_i - F_{t_i} r$ ,  $i = 1, 2, 3$  (see (3)). To obtain the generalized forces for  $\{X, Y, \Psi\}$ , we have to write the  $F_{t_i}$ ,  $i = 1, 2, 3$  acting at the wheels along the Cartesian degrees of freedom. This can be done by use of the matrix  $[R]^T$  [2]. Hence the six generalized forces can be written as

$$\mathcal{F} = \{r [R]^T (F_{t_1}, F_{t_2}, F_{t_3})^T, \tau_1 - F_{t_1} r, \tau_2 - F_{t_2} r, \tau_3 - F_{t_3} r\}. \quad (9)$$

The dynamic equations of motion for the WMR, including the effects of wheel slip, can be written as shown at the bottom of this page or compactly,

$$[M] \dot{\underline{V}} + \dot{\Psi} [Q] \underline{V} = r [R]^T \underline{F}_t \quad (10)$$

$$[I] \ddot{\underline{\theta}} + r \underline{F}_t = \underline{\tau}. \quad (11)$$

It may be noted that to arrive at the above equations, we have taken  $\{G\}$  and  $\{G'\}$  to be coinciding, i.e.,  $e_1 = e_2 = 0$ ,  $V_1 = \dot{e}_1$ ,  $V_2 = \dot{e}_2$  and  $L_1 = L_2 = L_3 = L$ . It may be noted that the term  $\dot{\Psi} [Q] \underline{V}$  arises because  $V_1$  and  $V_2$  are components along the moving  $X_{G'}$  and  $Y_{G'}$  axes and not along axis of the fixed coordinate system.

We can make the following observations from the dynamic equations of motion.

- The individual wheel dynamics are coupled with the WMR dynamics through the tractive forces. The ideal rolling condition is not used.
- The only input to this model of the WMR are the wheel torques,  $\tau_i, i = 1, 2, 3$ .
- The above equations of motion can be reduced to the equations of motion derived using the no slip conditions. This is shown below.

$$\begin{bmatrix} M_p & 0 & 0 \\ 0 & M_p & 0 \\ 0 & 0 & I_p \end{bmatrix} \begin{Bmatrix} \dot{V}_1 \\ \dot{V}_2 \\ \dot{\Psi} \end{Bmatrix} + \dot{\Psi} \begin{bmatrix} 0 & -M_p & 0 \\ M_p & 0 & 0 \\ 0 & 0 & 0 \end{bmatrix} \begin{Bmatrix} V_1 \\ V_2 \\ \dot{\Psi} \end{Bmatrix} = r [R]^T \begin{Bmatrix} F_{t_1} \\ F_{t_2} \\ F_{t_3} \end{Bmatrix}$$

$$\begin{bmatrix} I_1 & 0 & 0 \\ 0 & I_2 & 0 \\ 0 & 0 & I_3 \end{bmatrix} \begin{Bmatrix} \ddot{\theta}_1 \\ \ddot{\theta}_2 \\ \ddot{\theta}_3 \end{Bmatrix} + r \begin{Bmatrix} F_{t_1} \\ F_{t_2} \\ F_{t_3} \end{Bmatrix} = \begin{Bmatrix} \tau_1 \\ \tau_2 \\ \tau_3 \end{Bmatrix}$$

The wheel dynamics alone are given by (11). Multiplying (11) by  $[R]^T$ , and substituting for  $r [R]^T \underline{F}_i$ , from (10), we get

$$[R]^T [I] \ddot{\underline{\theta}} + [M] \dot{\underline{v}} + \dot{\Psi} [Q] \underline{v} = [R]^T \underline{\tau}. \quad (12)$$

The no-slip condition is given as  $\dot{\underline{\theta}} = [R] \underline{v}$ . Since  $[R]$  is a constant matrix, we obtain,  $\underline{\theta} = [R] \underline{v}$ , and on substituting them in (12) and rearranging, we recover the WMR ideal dynamic equations (see Agullo *et al.* [2]).

$$[M^*] \dot{\underline{v}} + \dot{\Psi} [Q] \underline{v} = [R]^T \underline{\tau} \quad (13)$$

where  $[M^*] = ([M] + [R]^T [I] [R])$ .

In this reduced order form, these equations are referred to as 'ideal' rolling equations.

## V. CONTROL OF THE WMR

The control problem for the WMR may be defined as that of guiding the WMR through a desired Cartesian path with specified terminal points. In this section, the path tracking performance of the WMR under PID control and a model based control using Cartesian space feedback is discussed. The Cartesian space feedback may be obtained either through dead reckoning or referential methods [6]. The dead reckoning method uses on-board sensors to estimate the current position of the WMR. In the present case, we assume that there are on-board sensors such as wheel encoders and accelerometers.

### PID Control

This control scheme uses the Cartesian space errors to compute the wheel torques according to the following PID control law

$$\underline{F} = K_v (\dot{\underline{X}}_d - \dot{\underline{X}}) + K_p (\underline{X}_d - \underline{X}) + K_i \int (\underline{X}_d - \underline{X}) dt \quad (14)$$

where  $\underline{X}$  denotes the vector  $(X, Y, \Psi)^T$  and  $\underline{X}_d$  is the desired Cartesian space path and  $(\cdot)$  denotes the derivative with respect to time.

The wheel torques,  $\underline{\tau}$ , are related to the Cartesian force,  $\underline{F}$ , and are given as

$$\underline{\tau} = [R]^T \underline{F}. \quad (15)$$

The dynamic model of the WMR is not used in this control scheme.

### Model-Based Control

The model based control approach seeks to exploit the model of the system to be controlled to obtain enhanced performance. The fundamental idea in this approach is to use the model of the system to be controlled in the control law, such that the resulting error equation is decoupled and linear, and is tunable by PID parameters [7]. In this section, we investigate the use of the dynamic equations of motion derived using the condition of 'ideal' rolling, (13) in the model-based control law. One possible rationale for using the 'ideal' rolling model is that it is very hard to model adhesion coefficient and other nonlinearities of the real system.

Assuming the availability of Cartesian space feedback and the reduced order 'ideal' rolling model, a model-based control law can be written as

$$\underline{\tau} = \alpha \underline{\tau}^i + \beta \quad (16)$$

where,

$$\begin{aligned} \alpha &= [R]^T [M^*] \\ \beta &= [R]^T \{ \dot{\Psi} [Q] \underline{v} \} \\ \underline{\tau}^i &= \ddot{\underline{X}}_d + K_v (\dot{\underline{X}}_d - \dot{\underline{X}}) + K_p (\underline{X}_d - \underline{X}) \\ \underline{X} &= \{ X, Y, \Psi \}^T \end{aligned}$$

where  $[M^*]$  is given in (13).

### Error Dynamics

The error dynamics for the WMR undergoing rolling with slip under the above model based control law is now presented. By substituting the expression for  $\underline{\tau}$ , (16), in (10) and (11) and rearranging, we get

$$\ddot{\underline{E}}_r + K_v \dot{\underline{E}}_r + K_p \underline{E}_r = \underline{f}_d(\dots, t) \quad (17)$$

where  $\underline{E}_r$  is the quantity  $(\underline{X}_d - \underline{X})$  and

$$\underline{f}_d(\dots, t) = [M^*]^{-1} [R]^T [I] \ddot{\underline{\theta}} + r [R]^T \underline{F}_i ([M^*]^{-1} - [M]^{-1}) - ([M^*]^{-1} - [M]^{-1}) C \quad (18)$$

where the quantities in the above equation are defined in Sections 4 and 5, and  $C$  denotes  $\dot{\Psi} [Q] \underline{v}$ .

We can consider the error equation as a linear system of second order ordinary differential equation subjected to a disturbance  $\underline{f}_d(\dots, t)$ . The first order representation of this system is given as

$$\dot{\underline{Y}} = - \begin{bmatrix} 0 & -I \\ K_p & K_v \end{bmatrix} \begin{Bmatrix} \underline{E}_r \\ \dot{\underline{E}}_r \end{Bmatrix} + \begin{Bmatrix} 0 \\ \underline{f}_d(\dots, t) \end{Bmatrix}$$

or compactly as

$$\dot{\underline{Y}} = -[A] \underline{Y} + D(\dots, t) \quad (19)$$

where,  $\underline{Y} = \{\underline{E}_r, \dot{\underline{E}}_r\}^T$ ,  $K_p$  and  $K_v$  are the positive definite gain matrices, and  $D(\dots, t) = \{0, \underline{f}_d(\dots, t)\}^T$  is the disturbance. It can be assumed that  $D(\dots, t)$  is bounded. For stability analysis, consider the following Lyapunov function

$$\mathcal{V} = 1/2 \underline{Y}^T \underline{Y}. \quad (20)$$

Differentiating with respect to time, we get

$$\dot{\mathcal{V}} = \underline{Y}^T \dot{\underline{Y}} = \underline{Y}^T (-[A] \underline{Y} + D)$$

For asymptotic stability  $\dot{\mathcal{V}} < 0$ , and we require

$$\|\underline{Y}\| > \|[A]^{-1} D\|. \quad (21)$$

The above condition implies that the ordinary differential equation will be asymptotically stable if the state vector,  $\underline{Y}$ , is of sufficient magnitude (greater than  $\|[A]^{-1} D\|$ ) to ensure that  $\dot{\mathcal{V}}$  is negative. Since  $D(\dots, t)$  is assumed to be bounded, the above equation suggests that  $\|\underline{Y}\|$  is bounded and will approach  $\|[A]^{-1} D\|$  as  $t$  tends to infinity. The analysis also suggest a possible limit cycle behavior since if  $\underline{Y} < \|[A]^{-1} D\|$  then the system may be unstable. The errors in WMR path tracking is clearly determined by the quantity  $\|[A]^{-1} D\|$ , and to reduce path deviation  $\|[A]^{-1} D\|$  must be made small. One way to make  $\|[A]^{-1} D\|$  small is by choosing large  $K_p$  and  $K_v$  which leads us to the (not surprising) conclusion that we can expect better performance from our controller by using larger gains. We can also reduce  $\|[A]^{-1} D\|$  by ensuring that  $D(\dots, t)$  is close to zero.

For  $D(\dots, t)$  to be zero, we must have

$$\underline{F}_i = 1/r ([M^*]^{-1} - [M]^{-1})^{-1} [R]^T \ddot{\underline{\theta}} - \{ ([M^*]^{-1} - [M]^{-1}) C - [M^*]^{-1} [R]^T [I] \ddot{\underline{\theta}} \}. \quad (22)$$

We can make the following observations from the above equation:

- For the disturbance  $D(\dots, t)$  to be zero, a minimum tractive force has to be developed ensuring rolling without slip. A higher adhesion coefficient ensures larger  $\underline{F}_i$  resulting in less slipping of the wheel and better Cartesian path tracking. This is observed in the simulations.
- Instances when the tractive force,  $\underline{F}_i$ , generated is insufficient may arise, resulting in a nonzero value for the disturbance,  $D(\dots, t)$ . This is the cause of roll/slip motion at the wheel and hence WMR path deviation.

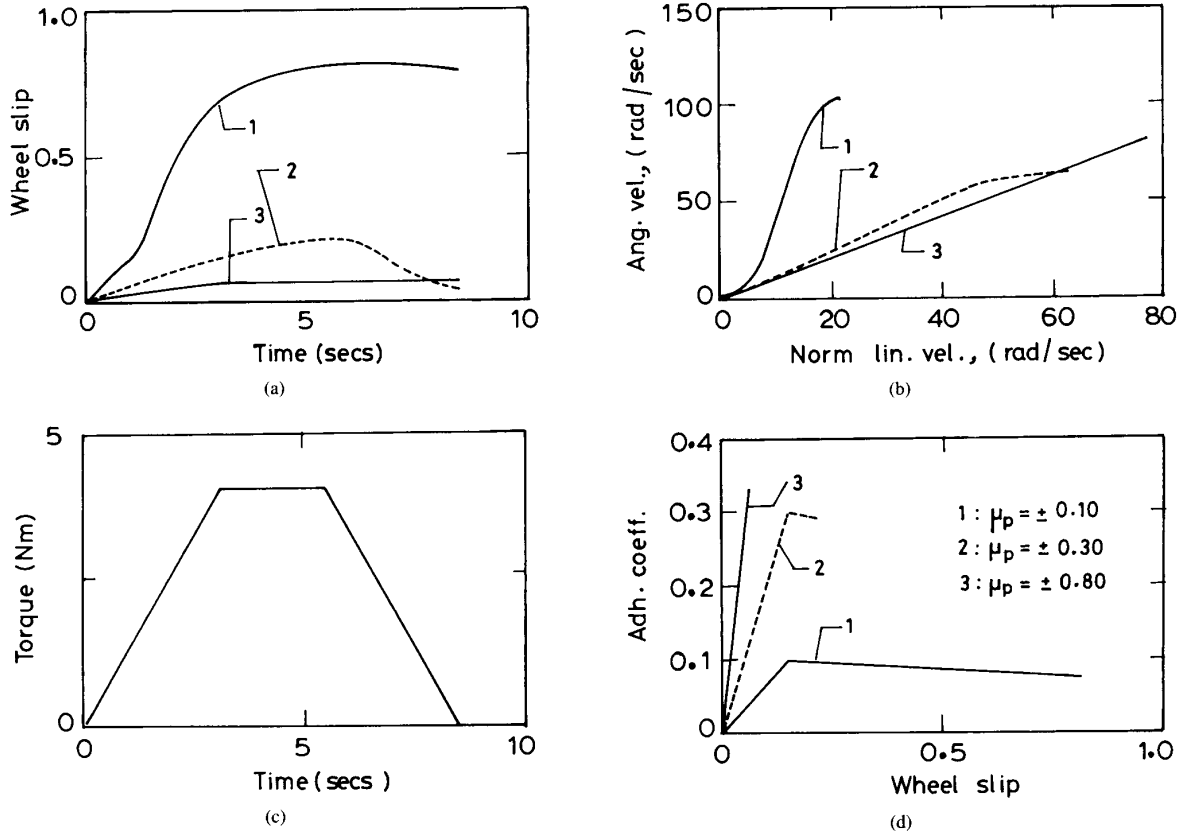


Fig. 4. Single wheel simulation.

- In general, the expression for  $f_d(\dots, t)$  may also contain external forces acting on the WMR. In such a situation, the required tractive force,  $F_T$ , is even larger and may not be sustained by the wheel and surface. This may result in WMR path deviation. This situation occurs during skidding.

From the above analysis, we can infer that for smaller WMR path deviation we have to use higher gains or ensure sufficient tractive force.

## VI. SIMULATION

In this section, we illustrate the effects of wheel slip on the motion of a single wheel and on WMR path tracking. In particular, we show that for a single wheel as the adhesion coefficient is increased conditions closer to 'ideal' rolling prevail. For the WMR, the performance of PID control is not satisfactory, and the use of 'ideal' rolling model, in model based control, is justified only for high values of adhesion coefficients, i.e., when conditions are closer to 'ideal' rolling.

For the purpose of simulation, the adhesion coefficient model was represented using the  $\mu_{a\_peak}$  as a parameter. Typically, a peak value of the adhesion coefficient,  $\mu_{a\_peak}$  is chosen to represent the surface roughness.  $\lambda_{a\_peak}$  is chosen to be  $\pm 0.15$ . For  $\lambda = \pm 1$ ,  $\mu_a$  was chosen to be  $0.66 \mu_{a\_peak}$ . The  $\mu_a$  versus  $\lambda$  curve is approximated by straight lines in the different regions and is given as

$$\mu = (\lambda - 0.15) \frac{\mu_{a\_peak}}{0.15} + \mu_{a\_peak}, \quad -0.15 < \lambda < 0.15$$

$$\mu = -(\lambda - 0.15) \frac{0.34\mu_{a\_peak}}{0.85} + \mu_{a\_peak}, \quad 0.15 \leq \lambda \leq 1.00 \quad (23)$$

$$\mu = -(\lambda + 0.15) \frac{0.34\mu_{a\_peak}}{0.85} - \mu_{a\_peak}, \quad -1.00 \geq \lambda \geq -0.15$$

The differential equations of motion were numerically integrated for obtaining simulation results. The equations were found to be "stiff" [13], especially for the cases where near rolling conditions were present. We used a "stiff" ODE solver based on the backward difference formula in [13].

### Single Wheel Dynamics

We first present a simple case, where a wheel is subjected to a trapezoidal torque profile with the peak adhesion coefficient,  $\mu_{a\_peak}$ , taking on values of 0.10, 0.30, and 0.80, respectively. The different values of peak adhesion coefficient,  $\mu_{a\_peak}$ , serves the purpose of representing surfaces of varying roughness and for a low  $\mu_{a\_peak}$  we expect a slipping as well as rolling motion. In this simulation, the wheel had a mass,  $M_w = 2.0$  kg and radius,  $r = 0.30$  m.

Fig. 4(a) shows the wheel slip variation with time. In Fig. 4(b), the plot of the normalized linear velocity,  $\omega^*$ , versus angular velocity,  $\theta$ , of the wheel is shown. Curves 1, 2, and 3 in Fig. 4(b) represent the plots for peak adhesion coefficient,  $\mu_{a\_peak}$ , values of 0.10, 0.30, and 0.80, respectively. It is observed that the plots deviate from the straight line which represents 'ideal' rolling. With decreasing adhesion coefficient the deviation from 'ideal' rolling shows an increase. For all the above cases the same trapezoidal torque profile, shown in Fig. 4(c), was used. Fig. 4(d) shows the variation of wheel slip,  $\lambda$ , and the adhesion coefficient  $\mu_a$ .

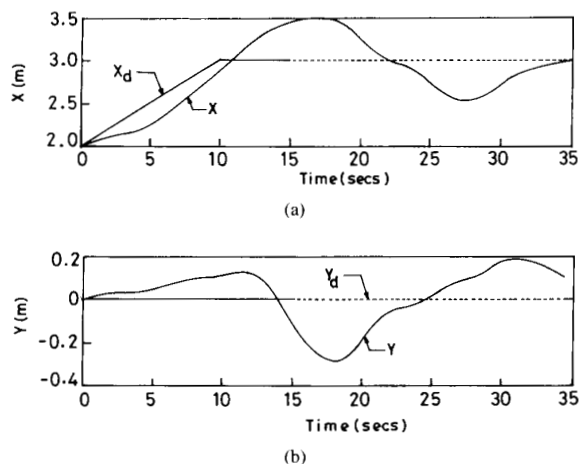


Fig. 5. Tracking performance with PID control.

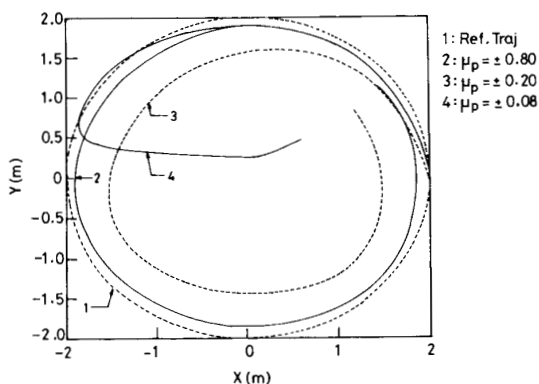


Fig. 6. Tracking performance with model-based control.

### WMR Simulation

The dynamic model of the WMR with the nonlinear effect of wheel slip, (10) and (11), were used in the simulation studies. The PID controller and the model based controller were used for simulation. The kinematic parameters of the WMR are  $L = 0.5m$ ,  $r = 0.1m$  and the wheels are at  $120^\circ$  to each other. The WMR dynamic parameters are,  $M_p = 50.0$  kg,  $I_p = 5.0$  kg  $m^2$ , and  $I_i = 2.0$  kg  $m^2$ ,  $i = 1, 2, 3$ .

#### Case 1 - Straight Line trajectory with PID control

The PID control law, (15), was used in a straight line trajectory. A peak adhesion coefficient,  $\mu_{peak}$ , value of 0.80 was used. The plot of the  $x$  and  $y$  co-ordinates with time are shown in Figs. 5(a) and 5(b), respectively. The following gains were used in the control law,  $K_p = 15.00$ ,  $K_v = 2\sqrt{K_p}$  and  $K_i = 0.10$ .

It can be observed that the tracking performance is quite poor.

#### Case 2 - Circular trajectory with Model Based Control

The WMR was made to track a circular Cartesian trajectory of radius 2 m centered about the origin. Different values of peak adhesion coefficient,  $\mu_{peak}$ , 0.80, 0.20, and 0.08, representing surfaces of decreasing roughness were taken. The simulation results show increasing path deviation with a decrease in the adhesion coefficient peak value  $\mu_{peak}$ . This is observed in Fig. 6. Plot 1 is the reference trajectory, plots 2, 3, and 4 are for  $\mu_{peak} = 0.80$ , 0.20, and 0.08, respectively.

To enable comparison of the tracking performance for the different simulations (commanded trajectory was a circle of radius = 2m, with

TABLE I  
CIRCULAR TRAJECTORY WITH MODEL-BASED CONTROL

S. No.	$\mu_{peak}$	$R_{error,max}$	$K_p$	$K_v$	$K_i$
1	0.80	0.15	2.00	$2\sqrt{K_p}$	0
2	0.20	0.58	1.00	$2\sqrt{K_p}$	0
3	0.08	1.71	2.00	$2\sqrt{K_p}$	0

center at the origin), the maximum radial error,  $R_{error,max}$ , given by,  $R_{error,max} = \max|R_{d,s} - R_a|$ , was used. For this case,  $R_{d,s} = 2$  m, and  $R_a = \sqrt{x^2 + y^2}$ ,  $(x, y)$  is the actual Cartesian position of the WMR. Table I shows typical values of  $R_{error,max}$ . It may be observed from Table I that higher peak adhesion coefficient,  $\mu_{peak}$ , values result in less deviation.

Other simulations were also performed with varying  $K_p$  for a given peak adhesion coefficient value and improvement in performance was observed with increased gain.

### VII. CONCLUSION

Most dynamic models of WMR do not incorporate the effects of wheel slip and traction. In this paper, we have shown that the wheel slip can have significant effect on the motion of a wheel, and the actual motion of the wheeled mobile robot is very much different from that obtained under 'ideal' rolling conditions.

The rolling and slipping as undergone by a wheel under tractive rolling were introduced through the use of traction models. The equations of motion of the WMR were obtained incorporating the effects of wheel slip. To illustrate the significance of slip, a PID controller and an 'ideal' rolling model based controller was used on a WMR model with slip. Simulation results show that the path errors are larger for lower adhesion coefficient values.

The analysis of the error equation suggest that the system is stable under certain conditions. Improved performance can be obtained by ensuring that the required tractive forces are available or by increasing controller gains. Numerical simulations of the WMR show that the performance in trajectory tracking with unmodeled slip and traction is not very satisfactory. The path deviation of the WMR is small only when the adhesion coefficient is chosen large representing conditions closer to "ideal" rolling. In conclusion, for better performance of a WMR, we have to model slip and use an accurate traction model.

### ACKNOWLEDGMENT

We wish to thank Rex J. Theodore for useful discussions on the present work. We also wish to thank the anonymous reviewers for their comments.

### REFERENCES

- [1] J. Agullo, S. Cardona, and J. Vivancos, "Kinematics of vehicles with directional sliding wheels," *Mechanisms and Machine Theory*, vol. 22, no. 4, pp. 295-301, 1987.
- [2] J. Agullo, S. Cardona, and J. Vivancos, "Dynamics of vehicles with directionally sliding wheels," *Mechanisms and Machine Theory*, vol. 24, no. 1, pp. 53-60, 1989.
- [3] J. C. Alexander and J. H. Maddocks, "On the kinematics of wheeled mobile robots," *Int. J. Robotics Res.*, vol. 8, no. 5, Oct. 1989.
- [4] R. R. Allen and R. C. O'Massey, "Longitudinal instability in braked landing gear," *Trans. ASME J. Dyn. Syst., Meas., and Cont.*, vol. 103, pp. 259-265, Sept. 1981.
- [5] C.-N. Chang and T.-T. Lee, "Stability analysis of three and four wheel vehicles," *JSME Int. J.*, Series III, vol. 33, no. 4, pp. 567-574, 1990.
- [6] I. J. Cox and G. T. Wilfong, Eds., *Autonomous Robot Vehicles*. New York: Springer-Verlag, 1990.
- [7] J. J. Craig, *Introduction to Robotics: Mechanics and Control*. Reading, MA: Addison-Wesley, 1986.

- [8] H. Dugoff, P. S. Fancher, and L. Segel, "An analysis of tire traction properties and their influence on vehicle dynamic performance," *SAE Trans.*, 1970.
- [9] S. Dwarakanath, B. Jayarajan, and A. Ghosal, "Design and fabrication of a mobile robot platform with omni-directional wheels," in *Int. Conf. Automat., Robotics and Comput. Vision*, (ICARCV '90), 1990.
- [10] A. Isidori, *Nonlinear Control Systems: An Introduction, Lecture Notes in Control and Information Sciences*. New York: Springer-Verlag, 1989.
- [11] P. F. Muir and C. P. Neuman, "Kinematic modelling of wheeled mobile robots," *J. Robotic Syst.*, vol. 4, no. 2, pp. 281-340, 1987.
- [12] P. F. Muir and C. P. Neuman, "Kinematic modelling for feedback control of an omni-directional wheeled mobile robot," in *Autonomous Robot Vehicles*, I. J. Cox and G. T. Wilfong, Eds. New York: Springer-Verlag, 1990.
- [13] L. F. Shampine and H. A. Watts, "DEPAC—Design of a user oriented package of ODE solvers," Report No. SAND79-2374, Sandia National Laboratories, Sept. 1980 (unpublished).
- [14] Z. Shiller and Y.-R. Gwo, in "Dynamic motion planning of autonomous vehicles," *IEEE Trans. Robotics and Automat.*, vol. 7, no. 2, pp. 241-249, Apr. 1991.
- [15] M. W. Spong and M. Vidyasagar, *Robot Dynamics and Control*. New York: Wiley, 1989.
- [16] H.-S. Tan and Y.-K. Chin, in "Vehicle traction control: variable structure control approach," *Trans. ASME, J. Dyn. Syst., Meas., and Cont.*, vol. 113, pp. 223-230, June 1991.
- [17] N. Matsumoto and M. Tomizuka, "Vehicle lateral velocity and yaw rate control with two independent control inputs," *Trans. ASME, J. Dyn. Syst., Meas., and Cont.*, vol. 114, pp. 606 - 613, Dec. 1992.
- [18] W. G. Unruh, "Instability in automobile braking," *Amer. J. Physics*, vol. 52, no. 10, Oct. 1984.
- [19] G. Wampfler, M. Salecker, and J. Wittenburg, "Kinematics, dynamics, and control of omni-directional vehicles with mecanum wheels," *Mechanical Struct. and Machines*, vol. 17, no. 2, pp. 167-177, 1989.

## Error Eliminating Rapid Ultrasonic Firing for Mobile Robot Obstacle Avoidance

Johann Borenstein and Yoram Koren

**Abstract**—This paper introduces error eliminating rapid ultrasonic firing (EERUF), a new method for firing multiple ultrasonic sensors in mobile robot applications. EERUF allows ultrasonic sensors to fire at rates that are five to ten times faster than those customary in conventional applications. This is possible because EERUF reduces the number of erroneous readings due to ultrasonic noise by one to two orders of magnitude.

While faster firing rates improve the reliability and robustness of mobile robot obstacle avoidance and are necessary for safe travel at higher speed (e.g.,  $V > 0.3$  m/sec), they introduce more ultrasonic noise and increase the occurrence rate of crosstalk. However, EERUF almost eliminates crosstalk, making fast firing feasible. Furthermore, EERUF's unique noise rejection capability allows multiple mobile robots to collaborate in the same environment, even if their ultrasonic sensors operate at the same frequencies.

We have implemented and tested the EERUF method on a mobile robot and we present experimental results. With EERUF, a mobile robot was able to traverse an obstacle course of densely spaced, pencil-thin (8 mm-diameter) poles at up to 1 m/sec.

Manuscript received June 1, 1992; revised July 1993. This work was supported in part by Department of Energy Grant DE-FG02-86NE37969 and in part by the Veterans Administration Grant 028085.

The authors are with the University of Michigan, Department of Mechanical Engineering and Applied Mechanics (MEAM), Ann Arbor, MI 48109-2110 USA.

IEEE Log Number 9403337.

## NOMENCLATURE

$a, b$	Index to alternating delays $T_{wait,a}$ or $T_{wait,b}$ .
$n, m$	Index to the $n$ th ( $m$ th) occurrence of an event.
$t_0$	Start of timing diagrams.
$t_{ct}$	The (absolute) time at which crosstalk occurred.
$x$	Sensor causing crosstalk, located at the beginning of a critical path.
$y$	Sensor affected by crosstalk, located at the end of a critical path.
$L$	Length of a critical path.
$T_\lambda$	Maximum allowable time difference between any two consecutive readings.
$T_{echo}$	Time from firing to receiving an echo.
$T_{err}$	Erroneous reading, caused by crosstalk.
$T_{fire}$	Amount of time from the beginning of a period to the actual firing of a sensor.
$T_{idle}$	Amount of time from receiving an echo to the beginning of the next period.
$T_{i,nom}$	Nominal time interval between scheduled firings of the sensors in a group.
$T_{i,min}$	Shortest time interval between actual firings of the sensors in a group.
$T_{lag}$	Amount of time a sensor is scheduled for firing after the beginning of a period.
$T_p$	Time period. The amount of time in which each sensor fires once.
$T_{wait}$	The amount of time EERUF waits before firing a sensor, after the sensor was already scheduled for firing.
$T_{wind}$	Time window—the amount of time a sensor is "open" to await an echo.
$T_{L,n}$	Amount of time soundwaves spend on traveling through the critical path.

## Abbreviations:

EERUF	Error Eliminating Rapid Ultrasonic Firing.
URS	Ultrasonic Range Sensor.

## I. INTRODUCTION AND BACKGROUND

This paper introduces error eliminating rapid ultrasonic firing (EERUF), a new method for noise rejection with ultrasonic range sensors (URS's). The EERUF method is designed to work with the widely used URS's manufactured by Polaroid [19]. A comprehensive discussion of the characteristics and limitations of these sensors can be found in the literature and is omitted here (see [1], [5], [10], [12], [15], [16]).

In order to guarantee complete coverage of the area around a mobile robot in all directions, many mobile robots have URS's installed on their periphery at  $15^\circ$  intervals.<sup>1</sup> For omnidirectional robots of circular shape, this design requires  $24 (=360^\circ/15^\circ)$  URS's mounted on a ring around the robot. Similar designs using 24 URS's in  $15^\circ$  intervals are described in the literature [17], [7], [2], [18], [9], [11], [6] and were used in the previously commercially available robot manufactured by Denning.

<sup>1</sup> Kuc [14] shows that theoretically it would be necessary to use even denser spacing (e.g.,  $5^\circ$ ) to cover all possible obstacles. However, we found that in practice  $15^\circ$ -spacing reliability detects obstacles as small as 8-mm-diameter vertical poles.